Cement and Concrete Research 39 (2009) 610–619

Contents lists available at ScienceDirect

Cement and Concrete Research

journal homepage: http://ees.elsevier.com/CEMCON/default.asp

Characterization of elastic and time-dependent deformations in high performance lightweight concrete by image analysis

Mauricio Lopez [a], Lawrence F. Kahn [b], Kimberly E. Kurtis [b,*]

[a] School of Engineering, Pontificia Universidad Católica de Chile, Av Vicuña Mackenna 4860, Casilla 306, Correo 22, Santiago, Chile
[b] School of Civil and Environmental Engineering, Georgia Institute of Technology, 790 Atlantic Dr. NW, Atlanta, Georgia 30332-0355, USA

ARTICLE INFO

Article history:
Received 28 May 2008
Accepted 27 March 2009

Keywords:
Aggregate
Cement paste
Creep
Interfacial transition zone
Shrinkage

ABSTRACT

Image analysis and strain mapping were used to examine the nature of elastic, creep and shrinkage strains in high performance lightweight concrete (HPLC). The strain maps showed non-uniform deformations related to microstructural features. Both average strain and non-uniformity increased with time under testing. Paste-rich regions exhibited higher creep plus shrinkage than the lightweight aggregate (LWA) particles examined herein; it is suggested that LWA could have a role in reducing deformations of the paste. Compared to normal weight high performance concrete (HPC), the paste and LWA in the HPLC exhibited more gradual spatial differences in elastic deformations, creep and shrinkage. It is proposed that this difference results from the lower stiffness of the LWA compared to granite used in the HPC. The results indicate that improvement in elastic property matching between the lightweight aggregate and high performance paste reduces stress concentrations at the aggregate/paste interface and contributes to reductions in deformations of HPLC compared to HPC.

1. Introduction

It is commonly understood that aggregate characteristics can strongly influence early and late age concrete properties such as workability, density, mechanical properties, and durability. Lightweight aggregate is not an exception; in addition to reducing the self-weight of concrete, the use of lightweight aggregate can influence other concrete properties. For example, it has been suggested [1] that lightweight aggregates, which possess lower stiffness than normal weight aggregates, exhibit an improved strain matching with paste during elastic deformation. This is believed to reduce microcracking at the aggregate/paste interfacial transition zone (ITZ) in normal strength lightweight concrete.

In low water-to-cementitious material ratio (w/cm) concretes, several researchers have concluded that the use of pre-wetted lightweight aggregates can improve overall concrete performance [2–5], reducing microcracking [6], enhancing hydration [7], decreasing autogenous shrinkage [8] and creep [9], improving durability [10], and enhancing the structure and properties in the ITZ [11,12].

Based on the still limited understanding of creep and shrinkage in concrete, the use of a relatively low stiffness aggregate (i.e., lightweight aggregate), instead of normal weight aggregate, should result in increased creep and shrinkage when all other mixture proportions and materials remain the same [13,14]. While this behavior is observed in normal strength lightweight concretes (20 to 30 MPa or 2900 to 4350 psi), it is *not* generally true in lightweight aggregate concrete with compressive strength of 35 MPa (5075 psi) or higher and especially in those used for high performance concrete (HPLC). That is, several studies [15–20] have reported lower creep and shrinkage in HPLC compared to HPC with similar mixture designs. Current understanding of creep and shrinkage is not enough to explain this apparent synergy between low w/cm high performance paste and pre-wetted lightweight aggregate in HPLC.

The objective of this research is to improve understanding of the influence of lightweight aggregate on deformation (i.e., elastic response, creep, and shrinkage) in HPLC — particularly as compared to similarly proportioned HPC containing normal weight aggregate. To better understand the fundamental differences in the interaction between the normal and lightweight aggregates and high performance paste, digital image correlation and strain mapping [21,22] were used to obtain local strain measurements in the aggregate, paste, and aggregate/paste interfacial transition region in HPLC and HPC after an initial application of stress and with sustained loading.

2. Experiment

Elastic strain, creep, and shrinkage were examined using digital image correlation to map deformation of HPLC and HPC concretes, prepared with identical proportions, but with different coarse aggregate (i.e., lightweight expanded slate vs. gneissic granite), as presented below.

2.1. Materials, mixture designs, and testing

Table 1 presents the mixture designs of the HPLC and HPC produced. The HPLC mixture design was based on Lopez et al. [17], with the maximum size aggregate (MSA) reduced to 9.5 mm (0.375 in.) for use in

* Corresponding author. Tel.: +1 404 385 0825; fax: +1 404 894 0211.
E-mail address: kkurtis@ce.gatech.edu (K.E. Kurtis).

0008-8846/$ – see front matter © 2009 Elsevier Ltd. All rights reserved.
doi:10.1016/j.cemconres.2009.03.015

Table 1
Mixture design of HPLC and HPC mixtures, kg/m^3 (lb/yd^3).

	HPLC	HPC
Type III Cement (75% of total cementitious materials)	442 (745)	442 (745)
Class F fly ash (15% of total cementitious materials)	89 (150)	89 (150)
Silica fume (10% of total cementitious materials)	59 (100)	59 (100)
Water	135 (228)	135 (228)
Natural siliceous sand (fineness modulus 3.15)	611 (1030)	611 (1030)
9.5 mm (0.375 in.) maximum size expanded slate	613 (1033)	NA
9.5 mm (0.375 in.) maximum size granite	NA	987 (1664)
Water reducer (0.45% of cementitious materials weight)	2.7 (4.6)	2.7 (4.6)
High range water reducer (1.00% of cementitious materials weight)	5.9 (9.9)	5.9 (9.9)
Air entrainer agent (0.05% of cementitious materials weight)	0.3 (0.5)	0.3 (0.5)
water-to-cementitious materials ratio (w/cm)	0.23	0.23
density kg/m^3 (lb/ft^3)	1958 (122.2)	2340 (146)

small-scale specimens used for imaging. The HPLC, with its w/cm of 0.23 and 590 kg/m^3 (995 lb/yd^3) of cementitious materials comprised of 75% Type III Portland cement, 15% Class F fly ash, and 10% silica fume, was meant to represent the type of mixture used in precast prestressed concrete application, where high early strength is desired. These cementitious factors along with the use of a natural siliceous sand fine aggregate were kept constant in the HPLC and HPC mixture designs.

For the HPLC, the coarse aggregate was a pre-wetted lightweight expanded slate. For the HPC mixture, the same volume of gneissic granite coarse aggregate, also with MSA of 9.5 mm (0.375 in.), was used. Table 2 shows the physical properties of the aggregate used in this study.

The small-scale specimens were 38×38×125 mm (1.5×1.5×5 in.) prism samples specially designed for imaging elastic, creep and shrinkage deformations. Additionally, 50.8-mm (2-in.) cube specimens and 38×38×125 mm (1.5×1.5×5 in.) prism specimens were cast from each mixture for measurements of compressive strength. All samples including those for creep, shrinkage, and compression testing were covered in their molds with polyethylene sheeting and were demolded after curing for 24 h. At that age, compressive strength specimens were tested, creep specimens loaded and stored together with shrinkage specimens at 50% RH and 23 °C (73 °F) in an environmental chamber for the duration of testing.

2.2. Mechanical testing

For each mixture, three cubes and three prisms were tested for compressive strength at 24 h of age, according to ASTM C 109 [23]. Measured compressive strengths are shown in Table 3.

Although the HPLC and HPC mixtures contained the same volume and type of cementitious materials and were produced at the same w/cm, the cube compressive strength of the HPC exceeded that of the HPLC by 19%. The compressive strength of HPLC was limited by the intrinsic strength of the expanded slate relative to granite [18,20,24,25].

As expected, the cube compressive strength was higher than that measured on the prisms for both HPLC and HPC specimens because of their differences in geometry. Since the geometry of the prisms corresponded to the geometry of the specimens to be used in this investigation for imaging, the 24-hour strength from the prisms was used to determine the stress to be applied to the creep specimens.

Table 2
Aggregate properties.

Type	Expanded slate	Granite	Siliceous sand
Maximum size aggregate, mm (in.)	9.5 (0.375)	9.5 (0.375)	2.5 (0.01)
Relative density (SSD)	1.560	2.681	2.513
Relative density (oven dry)	1.447	2.665	2.510
24-hour absorption (%)	7.8	0.6	0.1

Table 3
Compressive strength and applied stress in HPLC and HPC mixtures in MPa (psi) at the age of 24 h.

	HPLC	HPC
Compressive strength (cubic specimens)	64.8 (9400)	77.0 (11,165)
Compressive strength (prismatic specimens)	45.2 (6552)	67.8 (9835)
Applied stress to creep specimens (prismatic specimens)	21.0 (3040)	28.4 (4115)

2.3. Creep and shrinkage measurements and imaging

The HPLC and HPC creep specimens were placed in the small-scale frames (described below) and were loaded to approximately 44% of their respective 24-hour compressive strengths. Subsequently, both creep and shrinkage specimens were stored in an environmental chamber as described above.

Digital images and Detachable Mechanical (DEMEC) strain gauge readings (accurate to 0.0025 mm/0.0001 in.) were made before and immediately after application of load, and then after one and 28 days under loading and drying. The companion shrinkage specimens were installed in a similar frame, kept at the same environmental conditions, but remained unloaded. Images and DEMEC readings were obtained from the shrinkage specimens in the same fashion as the creep specimens. Additionally, DEMEC readings for the creep and shrinkage specimens were taken at seven and 120 days after loading.

2.3.1. Experimental setup

The experimental setup consisted of the small-scale specimen with an axial compression system that allowed for both sustained loading and digital imaging over time. This setup consisted of an internal 862-MPa (125-ksi) yield strength steel rod under tension and a prismatic concrete specimen under compression. The setup followed the guidelines provided by ASTM C 512 [26], but it contained the reduced size 38×38×125 mm (1.5×1.5×5 in.) prism specimen. This allowed the sample and test frame system to fit on the sample stage of a stereomicroscope for digital imaging. The system was reloaded periodically to maintain constant stress on the specimens.

Two specimens were created from a single cast sample after demolding and initial curing by sawing the sample in two. The saw cut eliminated edge effects from sample casting and created a surface with exposed aggregate. The flat sawn surfaces were polished using 120, 240, 360, and 600 silicon carbide (SiC) grits.

Fig. 1a shows the small-scale creep frame in the indexible stereomicroscope stage while an image is acquired. Also shown are some prisms after sawing and polishing (Fig. 1b), including one where the cast hole for the tensioned steel rod is visible. The experimental setup, procedures, and the image analysis methodology are described in greater detail elsewhere [21,22].

2.3.2. Imaging procedure

Four regions of interest (ROI) were examined on each specimen using two levels of magnification. At the lower magnification (termed "low" magnification herein), which corresponded to 12.6× through the eyepieces, one pixel represented 5.92 μm (2.3×10^{-4} in.). At "high" magnification, which corresponded to 80× as seen through the eyepieces, one pixel represented 1.08 μm (4.2×10^{-5} in.). ROIs were selected to contain aggregate, paste, and aggregate/paste interfacial region to characterize strain in each of the different phases.

2.3.3. Pattern matching procedure and strain mapping

The prisms were oriented during imaging such that the horizontal direction in the images acquired corresponded to the loading direction. Once the images were acquired, a pattern matching procedure was applied to compare image pairs obtained at the same ROI but at different states of deformation. Each pair of images had a "reference image" (REF) and a "deformed image" (DEF). Commercially

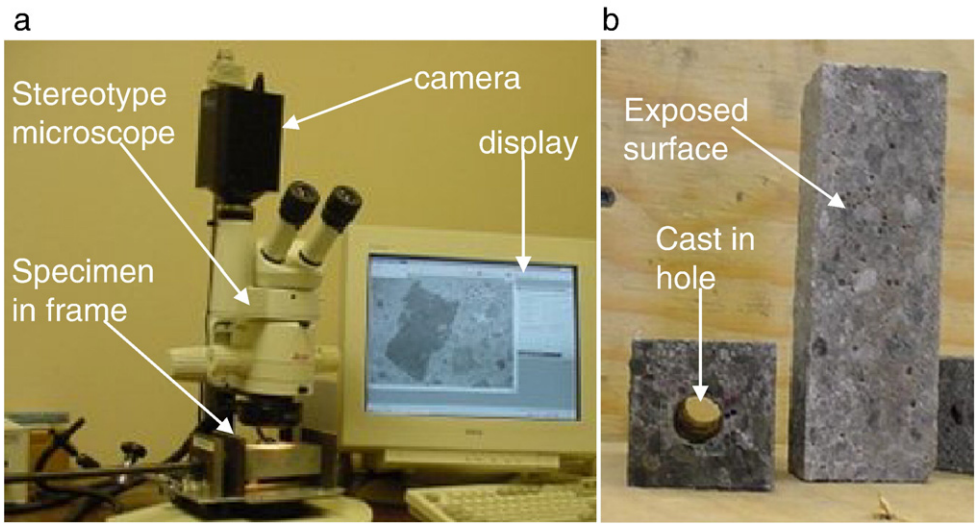

Fig. 1. (a) Image acquisition system, creep frame, specimens, stereomicroscope stage, digital camera, and computer, (b) Concrete prismatic specimens after cutting and polishing.

available software with pattern recognition capabilities [27] was modified with a C-script [21] to scan through the image pair to locate the coordinates of 6072 pixels (called matched pixels) in both REF and DEF images.

Once the coordinates of all the matched pixels were known in both images, another C-script [21] calculated the displacement in the loading direction as the difference in the horizontal coordinates of the matched pixels in the REF and DEF images. The strain was computed as the relative displacement between two matched pixels; i.e., as the difference in displacement divided by the original distance between pixels (15 pixels) [21,22].

After image acquisition and data processing, strain maps of the ROIs were generated using the computed strains and the original coordinates of each matched pixel. The maps represent localized strain measurements which can be visually related to the different phases or features present in the ROI and can be averaged to estimate the bulk strain measurement of the ROI.

3. Results

The relative behavior of HPLC and HCP were compared through compressive strength, creep and shrinkage testing and through analysis of images showing elastic deformations as well as creep and shrinkage deformations at different times of testing. The results help to better understand the interaction between the lightweight and normal weight aggregates and high performance paste during deformations of concrete.

3.1. Validity of approach

While the validity and accuracy of the digital image correlation and strain mapping employed here have been previously demonstrated [21,22], it is nevertheless worthwhile to compare the measurements of creep and shrinkage obtained via image analysis to those bulk measurements made using the DEMEC gauge on these HPLC and HPC samples.

To compare results from such different measuring systems, the strain maps had to be averaged into a single strain value that represents the bulk strain of the ROI. Fig. 2 compares the elastic, creep and shrinkage average strains from the strain maps with those measured using the DEMEC gauge. The diagonal gray dashed line in Fig. 2 represents the equivalence between strains obtained by the two systems.

Comparing both measuring systems — strain maps and DEMEC gauges — shows that the average strains from the DIC and bulk data followed the same trend. Moreover, the proximity to the equivalence line suggests that the two systems gave similar results. Considering all data points, the strains from DEMEC reading were about 25% higher than average strains from strain maps. This difference may be expected, however, since the ROIs were carefully selected to map strains in the aggregate, paste and their interface and not to image an area where the relative exposed surfaces of the phases present necessarily represented the actual proportions in that sample. Therefore, knowing that creep is directly related to the amount of paste present [13], ROIs containing a lower paste fraction, relative to the actual mixture proportions, would show lower strains. This, in addition to the fact that the gauge lengths of the strain maps — ranging from 1.5 to 8.3 mm (0.06 to 0.32 in.) — were much smaller than those for DEMEC gauge (127 mm/5 in.), also explains part of the variability of the image analysis method seen in Fig. 2.

In addition to the comparison shown in Fig. 2, the pattern matching procedure was tested against rigid body motion [21]; i.e., two images of the same ROI were taken before and after applying a known displacement using the indexible microscope stage to displace all the pixels of the ROI by the same amount. After running the pattern matching algorithm and computing the displacements, it was found that there was a difference in displacements between pixels; however, this difference was less than 0.25 pixels which, at the higher magnification used in this research,

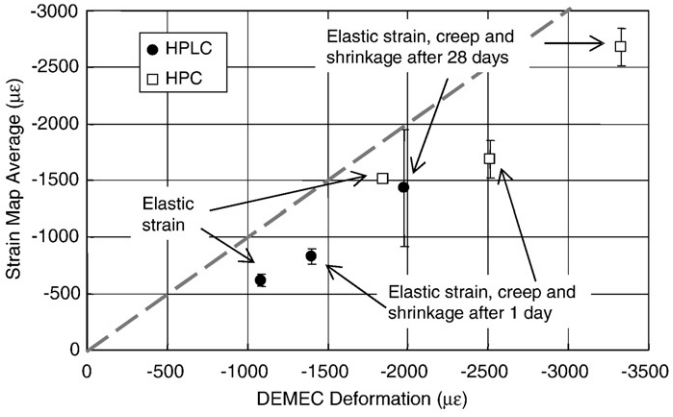

Fig. 2. Total strain measured from strain maps versus strain measured using DEMEC gauge.

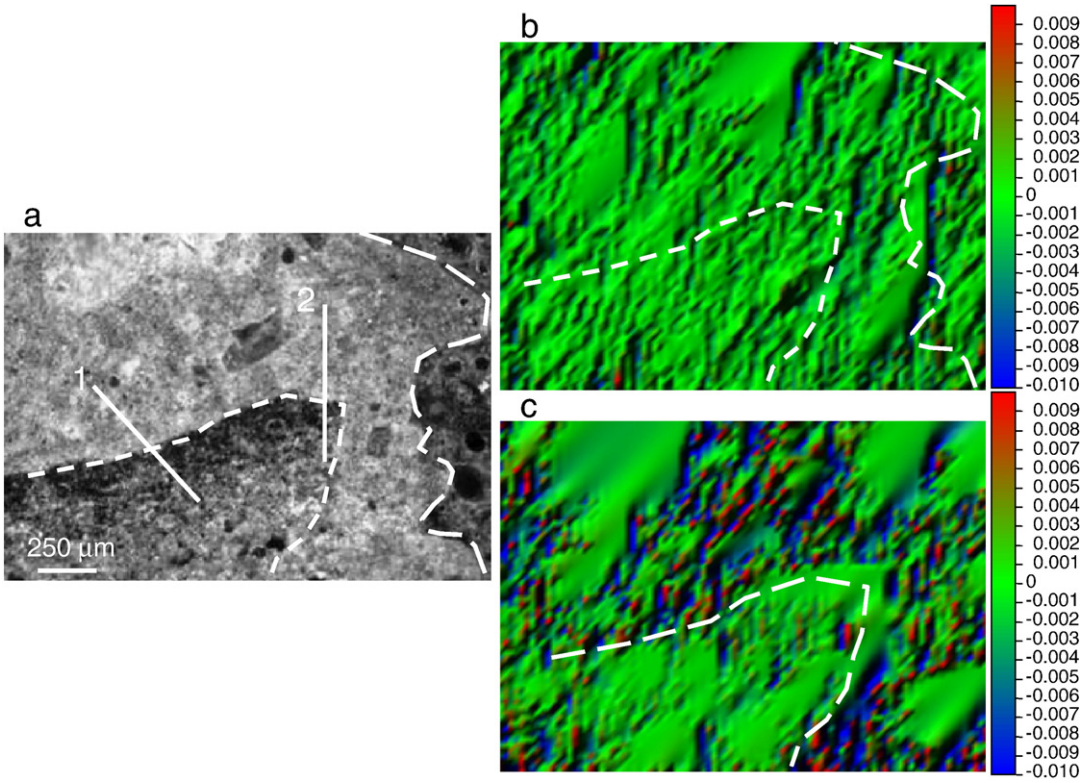

Fig. 3. (a) A representative region of interest (ROI 2), obtained at high magnification on an HPLC specimen. (b) A strain map of this ROI, showing elastic deformations, in the loading direction, in mm/mm (in./in.). (c) A strain map of this ROI, showing deformation due to creep and shrinkage after 28 days, in the loading direction, in mm/mm (in./in.). (For interpretation of the references to color in this figure legend, the reader is referred to the web version of this article.)

represented differences of 0.28 μm (1.05×10^{-5} in.), which was considered to be acceptable for this investigation.

3.2. Deformation in HPLC

3.2.1. Elastic strain in HPLC

As previously described, the prismatic HPLC specimens were loaded at 24 h with a stress of 21.0 MPa (3040 psi). Comparing images obtained prior to and just after loading shows the elastic strain distribution in the various ROIs imaged. Fig. 3 shows one region (ROI 2 in Fig. 3a) and the corresponding elastic strain map (Fig. 3b), obtained from the pattern matching between images taken immediately before and after loading (Fig. 3 also shows the 28-day creep plus shrinkage strain map of the same ROI which will be discussed in the following section).

The elastic strain map (Fig. 3b) shows a range in deformations between 10,000 με in tension (represented by red) and −10,000 με in compression (represented by blue), with 88% of the pixels experiencing elastic strain between 3000 and −4000 με, as shown by the predominantly bluish green color in the map. Tensile strains in a compressive stress field might be produced by Poisson's effect in the presence of different material components (i.e., paste, aggregate) and by discontinuities in the stress/strain field due to the presence of inclusions with variable properties (e.g., hard, stiff aggregates vs. voids). As a reminder, these inclusions can also exist below the imaged surface. Overall, the strain map shows a heterogeneous elastic deformation throughout the HPLC microstructure.

A non-uniform elastic strain field was also observed in the strain maps obtained for the other three ROIs (not shown) on this HPLC sample. The heterogeneity in the elastic response results from the heterogeneous HPLC microstructure itself, which is comprised of lightweight coarse aggregate, siliceous sand, cementitious paste and voids. Results indicating non-uniformity were obtained previously for the elastic response of normal weight, normal strength concrete, which is, of course, also heterogeneous in its composition [22,28].

Although the elastic strain field was non-uniform, the average elastic strain in the loading direction, considering the 6072 matched pixels, was compressive, measuring −557 με, for ROI 2 (Fig. 3b). Likewise, the average strains from the other three maps (ROIs 1, 3 and 4) on this sample were −680, −604 and −622 με. Therefore, despite measurements which indicate that sub-regions were experiencing tensile strain, the strain maps consistently indicated a compressive strain field, as would be expected from the applied compressive stress.

When further comparing the elastic strain map to the microstructural features of the ROI in Fig. 3a, it can be concluded that lightweight aggregate and paste largely elastically deform together. That is, there is no evidence of differences in deformations in the paste-rich regions and the aggregate-rich regions, which are indicated by dashed lines in Fig. 3. This highlights an important difference with respect to elastic deformation in normal weight concrete as previously reported [22] where important differences in elastic strains in aggregate and the paste were observed. This improved elastic matching between lightweight aggregate and paste was postulated for normal strength lightweight concrete [1,6], based on analytical elasticity calculations and mechanical properties of aggregate and paste; however, to the authors' knowledge this is the first experimental evidence demonstrating the enhanced strain matching between lightweight aggregate and paste. These results demonstrate that the elastic matching exists in a high performance/high strength paste containing this type of lightweight aggregate, and it can be expected that the same might happen with a lower strength/lower stiffness paste (i.e., normal strength lightweight concrete).

3.2.2. Creep and shrinkage strain in HPLC

Creep and shrinkage strains in HPLC were mapped using the same experimental setup, pattern matching, and calculation procedure used for obtaining the elastic strain maps. Here, however, the image taken immediately after loading was used as the “reference (REF)” image

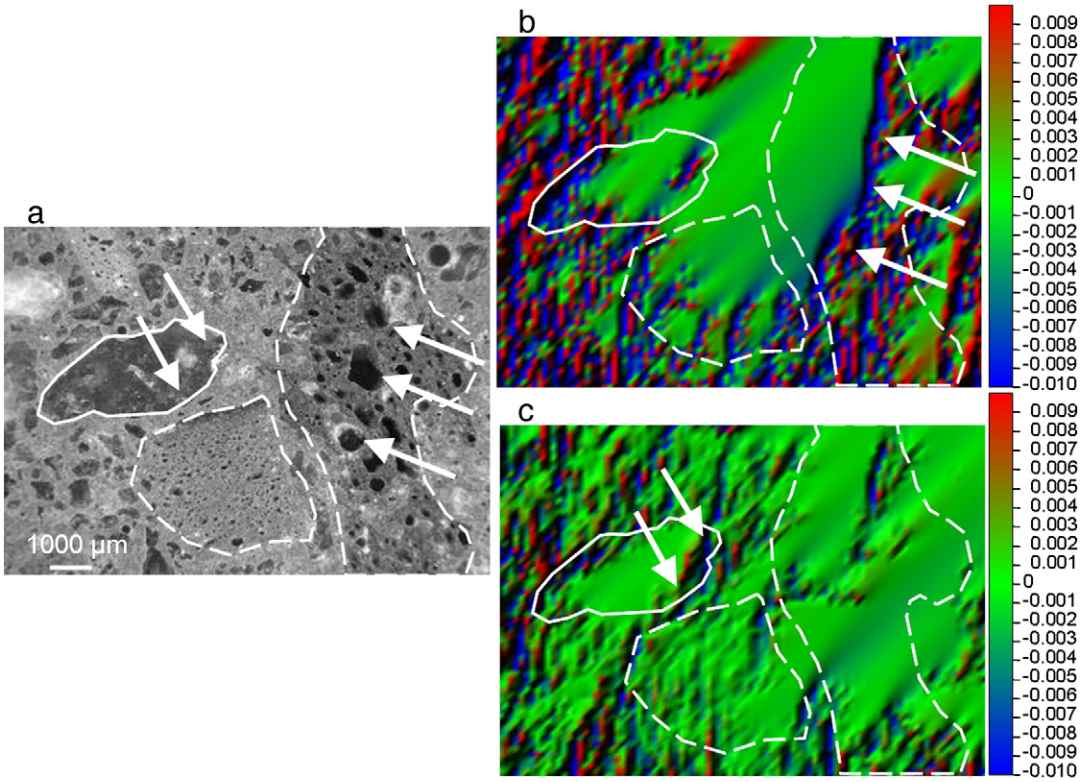

Fig. 4. (a) A representative region of interest (ROI 1), obtained at low magnification on an HPLC specimen. (b) A strain map of this ROI, showing deformation due to creep and shrinkage after one day, in the loading direction, in mm/mm (in./in.). (c) A strain map of this ROI, showing deformation due to creep and shrinkage after 28 days, in the loading direction, in mm/mm (in./in.). (For interpretation of the references to color in this figure legend, the reader is referred to the web version of this article.)

and the images taken after either one or 28 days under sustained loading and drying were used as the "deformed (DEF)" images.

Fig. 4a presents ROI 1 at low magnification and Fig. 4b the strain map obtained after one day under loading and drying for an HPLC specimen. The same scale in the creep and shrinkage map (10,000 με in tension, red, to −10,000 με in compression, blue) as in the elastic strain map. However, deformations were generally lower, with nearly 70% of the pixels deformed between +1000 and −1000 με, and with an average creep plus shrinkage strain of −179 με at one day. Even though the deformation map had both tensile and compressive strain regions, the average deformation from the maps was always negative (compression) for the four ROIs examined. The presence of tensile strain sub-regions on a specimen under compressive stress are believed to result from heterogeneities in the microstructure, as suggested previously by others [29,30] observing cement paste during drying shrinkage.

Unlike the elastic deformation in HPLC (see Fig. 3b), where the lightweight aggregate and high performance paste deformed together, the creep plus shrinkage maps in Figs. 3c and 4b and c show non-uniform, time-dependent deformation, with differences between aggregate-rich and paste-rich regions. For instance, the center region in this ROI (Fig. 4a), which includes some coarse aggregate particles, showed less creep plus shrinkage strain than the surrounding paste-rich region. In addition, the strain pattern in the central aggregate-rich region appears "smoother" or more homogeneous. While a high compressive strain region is apparent as a vertical line through the lightweight aggregate to the right of the "smooth" region (see arrows in Fig. 4b), that line of relatively high deformation might have been caused by the presence of uncommonly large pores in the aggregate particle, as highlighted by the arrows in Fig. 4a.

Elastic deformations occur instantaneously (or nearly so) in both paste and aggregates, with the strain distribution dependent upon the relative stiffness of each component. Creep plus shrinkage deformations, on the contrary, are time-dependent and largely originate in the paste; therefore, the aggregate — being the more creep and shrinkage-resistant phase — experiences significantly smaller deformation during creep and shrinkage and can act to restrain the creep and shrinkage of the paste [13,14]. It should be noted that the strain in the paste and aggregate shown in Fig. 4b does not include the initial elastic strain of the ROI.

It is believed that the increased strain observed in the aggregate after 1 day of loading and drying (Fig. 4b), does not result from creep and shrinkage but from delayed elastic deformation due to stress redistribution. As paste undergoes creep and shrinkage, it decreases its relative stiffness and transfers compressive force to the aggregate which consequently exhibits more elastic strains [31].

For ROI 1 a non-uniform strain field was apparent for creep plus shrinkage also after 28 days (Fig. 4c), with differences in deformation between aggregate and paste. The top-left, left and bottom areas of the map, which are paste-rich sub-regions, showed greater heterogeneity in their strain after 28 days, as evident by more contrast between bluish and reddish green zones which represent compressive and tensile strains. The average strain after 28 days was −428 με for ROI 1, with nearly 70% of the values lying between +2500 and −2500 με. This average strain at 28 days was 2.4 times larger than measured for the same ROI at one day of loading. The large strain shown by the arrows in Fig. 4b was reduced after 28 days under testing (Fig. 4c) which might indicate some relaxation.

ROI 1 included paste-rich zones, lightweight aggregate (indicated by dashed lines), and also normal weight fine aggregate (indicated by a solid line border) in Fig. 4. The creep and shrinkage map shows the difference between the influence of the lightweight and normal weight aggregates on the deformation field. The normal weight aggregate exhibits a more uniform deformation relative to the paste surrounding it, while the strain map within the lightweight aggregate is less uniform. Nonetheless, overall, the lightweight aggregates experienced lower deformations than the surrounding paste. In fact, the two lightweight particles (highlighted with dashed lines), and the

paste between them, seem to act together as one zone of low deformation. This suggests a restraining effect of the lightweight aggregate for creep and shrinkage occurring in the paste and also suggests improvements in the lightweight aggregate/paste interfacial region.

In contrast, the normal weight aggregate/paste interfacial region next to the normal weight aggregate (see downward arrows in the strain map in Fig. 4c) showed greater deformation than the paste lightweight aggregate/paste interfacial region. This higher deformation near the interface with the normal weight aggregate might be due to the greater difference in stiffness between the paste and such aggregate. This deformation map suggests that the lower stiffness of the lightweight aggregate, together with its improved aggregate/paste bonding [11,12], better accommodates the deformation mismatch between aggregate and paste, leading to less deformation in the high performance paste adjacent to the lightweight aggregate.

Examining creep plus shrinkage of another HPLC ROI, at higher magnification (Fig. 3), supports the observations made on the lower magnification images (Fig. 4). For example, the creep plus shrinkage strain map for ROI 2 HPLC after 28 days (Fig. 3c) shows non-uniform strain field with regions under compressive and tensile strains, where time-dependent deformations are more concentrated in the paste-rich zone (bluish green) while the aggregate experienced lower and less heterogeneous strains (reddish green).

The average creep plus shrinkage from two paste-rich sub-regions within ROI 2 were −1631 and −2095 με. The average strain considering the entire ROI (including both paste and aggregate) was −1128 με. This shows that the paste-rich zones exhibited considerably higher creep plus shrinkage deformation than the paste and aggregate together. This difference in strains further supports the restraining effect of the lightweight aggregate in creep and shrinkage occurring in the paste. In fact, this restraining role can be observed in the decreased strains in the paste immediately surrounding the lightweight aggregate (see dashed line in Fig. 3c).

Maps of creep plus shrinkage strain were also made for the same ROIs after 28 days of loading and drying as shown in Fig. 3c for ROI 2 and in Fig. 4c for ROI 1. It should also be noticed that the average 28-day creep plus shrinkage measured by image analysis was 40% higher for ROI 2 than for ROI 1, although both ROIs were from HPLC. This difference is likely related to the difference in composition of the two ROIs. Specifically, the higher magnification ROI 2 included a greater area fraction of paste than ROI 1. Thus, a greater average strain would be expected in ROI 2 than in ROI 1.

3.2.3. Creep and shrinkage in HPLC at one day versus 28 days

Comparing the deformation maps for ROI 1 at one and 28 days loading and drying (Fig. 4b and c), some redistribution of the strain over time is evident. For example, the center-top paste-rich subregion of Fig. 4a, which seemed to act together as one zone of low deformation at 1 day (Fig. 4b), shows higher and more heterogeneous deformations at 28 days of loading. Also, the larger lightweight aggregate particle which presented comparatively large deformations after one day, showed lower values after 28 days, suggesting that the aggregate recovered some of the initial high localized strain as paste underwent creep and shrinkage. Also, by quantitatively comparing strain maps for the same ROI from Fig. 4b and c, it can be concluded that the average strain increased between one and 28 days of testing, as did the strain distribution.

Fig. 5 presents a comparison of the strain distribution between one and 28 days of testing in a frequency plot. After one day of testing, 83% of the pixels presented strains between +2000 and −2000 με, as represented by the two largest black bars. After 28 days, the percentage of pixels with strains between +2000 and −2000 με was just 53%, with a clear increase of the percentage of pixels with higher strains. This change with time of loading and drying can be seen clearly by comparing the wider distribution of gray bars to the narrower distribution of black bars in Fig. 5. Also, high compressive strains increased more than high tensile strains, making the average strain shift toward more compressive values as duration of loading and drying increased.

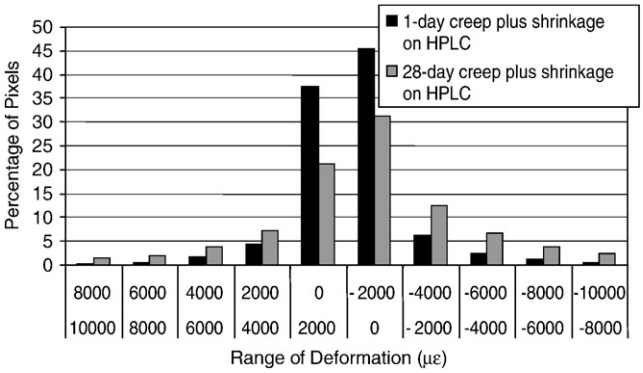

Fig. 5. Strain distribution after one and 28 days under loading and drying in ROI 1 at low magnification of HPLC specimen.

The increase in non-uniformity with time can be also observed when comparing the standard deviations from the strain measurements for each map. The standard deviation after one day under loading and drying was 2457 με while after 28 days it increased to 4578 με. The increase standard deviation might be viewed as a quantitative manifestation of the dissimilar time-dependent behavior of the paste and aggregate. Thus, the difference between the strain occurring in the aggregate and that in the paste became more pronounced as time under loading and drying increased.

3.3. Deformation in HPC

The elastic and creep plus shrinkage behavior observed in the companion HPC is concisely described below and will be subsequently compared with the HPLC. However, a more detailed presentation and analysis of the deformation behavior in this HPC can be found in [21,22], where the deformation in HPC relative to normal strength concrete (NSC) was considered.

3.3.1. Elastic strain in HPC

The strain map for the elastic deformation in a ROI at high magnification (shown in Fig. 6a) in a HPC sample is presented in Fig. 6b. A heterogeneous elastic strain field is apparent, with some regions in tension, but with most of the ROI in compression. The average elastic strains from the strain map was −1533 με (i.e., compressive).

The strain map is clearly related to microstructural features in the ROI for this HPC. For example, the coarse aggregate particle at the center of the ROI exhibited smaller strain and less heterogeneity in its elastic response than the surrounding paste; similar behavior is apparent at two other aggregate-rich sub-regions, at the upper left of the ROI (Fig. 6a). The lower part of the strain map, which is paste-rich, indicates greater strain. This variation in elastic response to the application of stress by the paste and aggregate is likely due the elastic mismatch between these two phases. This elastic mismatch could have induced microcracking at the aggregate/paste interface, indicated by a narrow high-strain band adjacent to the coarse aggregate and denoted by arrows in Fig. 6b. It may be recalled that no apparent mismatch was observed in the elastic strain map of HPLC (Fig. 3b).

3.3.2. Creep and shrinkage strain in HPC

The strain map for the deformation due to creep plus shrinkage after 28 days in a ROI at high magnification in a HPC sample is presented in Fig. 6c. The creep and shrinkage map shows generally lower strain values (reddish green) than those in the elastic strain map (Fig. 6b).

In general, creep and shrinkage strains in the HPC were greater and more heterogeneous in the regions with less coarse aggregate. For

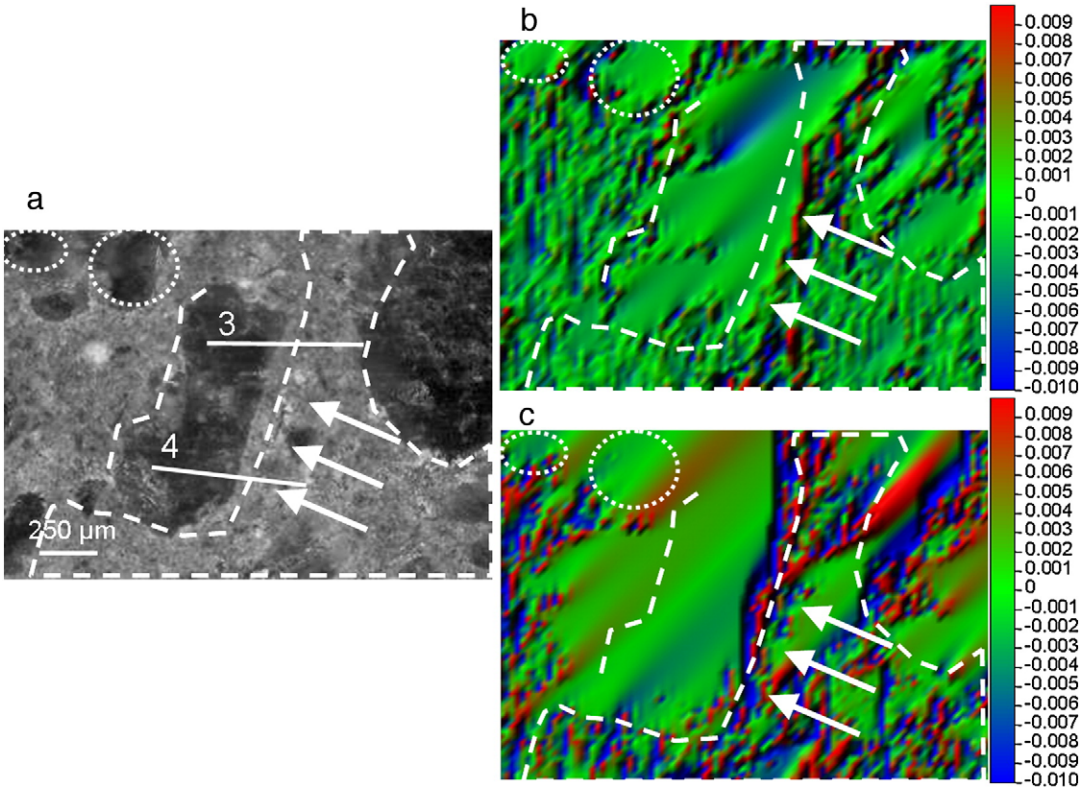

Fig. 6. (a) A representative region of interest, obtained at high magnification on an HPC specimen. (b) A strain map of this ROI, showing elastic deformations, in the loading direction, in mm/mm (in./in.). (c) A strain map of this ROI, showing deformation due to creep and shrinkage after 28 days, in the loading direction, in mm/mm (in./in.). (For interpretation of the references to color in this figure legend, the reader is referred to the web version of this article.)

example, the aggregate-rich sub-regions in the center and upper left of the image appear "smoother" and less heterogeneous, exhibiting less compressive strain than the paste fraction in this HPC ROI. The average creep plus shrinkage in the paste-rich zones was −2046 με, which is 80% higher than the strain of −1136 με measured in the paste and aggregate combined, indicating the paste is the predominant source of time-dependent strain in this HPC, as was the case for the HPLC.

Furthermore, as previously discussed [22] an aggregate restraining effect on paste creep and shrinkage in HPC may be visually apparent as a larger "smoother" area at the center of the ROI after creep and shrinkage (Fig. 6c) relative to the same region just after loading (Fig. 6b). In Fig. 6c, the lower strain region encompasses not only the aggregate, but some of the surrounding cementitious matrix as well.

Another feature of note in this HPC ROI is the region of high-strain detected along the right edge of the aggregate particle at the center of ROI (see arrows in Fig. 6c). This high-strain line, which is even more evident at 28 days of loading and drying, may indicate cracking or crushing along the aggregate/paste interfacial region. It should be noted that the high-strain zone shown in Fig. 6c does not include the elastic strain shown in Fig. 6b.

Detailed examination of a paste-rich region (lower right in Fig. 6c) shows higher and more heterogeneous strain than in the aggregate, suggesting that creep and shrinkage originates in the paste. As such, the aggregate particles at the center and at the top left corner — delimited by the dashed line — presented less strain than the paste-rich zone.

Assuming that the normal weight coarse aggregate experiences negligible creep and shrinkage [32], the time-dependent deformations exhibited by the granite in HPC are most probably due to a delayed elastic deformation. As the relative stiffness of the paste decreases due to its creep and shrinkage, the load carried by the aggregate consequently increases producing a delayed elastic deformation.

The arrows in Fig. 6c highlight the large strains obtained in the aggregate/paste interfacial region. The contact zone between paste, which undergoes creep and shrinkage, and the rigid normal weight aggregate particle, which does not undergo creep and shrinkage, presents an important strain mismatch. Such strain mismatch might even develop microcracking as suggested in the strain map. This was also observed in Fig. 4c with the siliceous sand particle (normal weight aggregate) present in the ROI of the HPLC specimen.

Comparing the creep and shrinkage strain maps at one and 28 days [22], shows that as time under loading and drying increased, the number of pixels in compression also increased in this HPC. Not only did the average strain increase between one and 28 days, but the standard deviation also increased by a factor of 3.5. It was proposed [22] that the increase in standard deviation in the strain measurements with time, coupled with the observations of lower strain and more homogeneity in strain measurements in the aggregate-rich subregions, may be viewed together as an indication that the creep and shrinkage occur primarily in the HPC paste, with the largest strains generally evident in the paste near the aggregate/paste interfacial region.

4. Discussion: Comparison between HPLC and HPC

Variations in elastic behavior and creep and shrinkage deformation between these similarly proportioned concretes will be compared using the strain maps obtained for HPLC (Fig. 3) and those obtained for HPC (Fig. 6). The maps were obtained at the same magnification, following the same image acquisition and image analysis procedures.

4.1. Elastic strain

HPLC presented a heterogeneous elastic strain map that did not show clear differences between paste-rich and aggregate-rich subregions. On the contrary, HPC presented an elastic strain field with marked differences between paste-rich and aggregate-rich subregions, suggesting that the applied stress is distributed differently between phases according to their

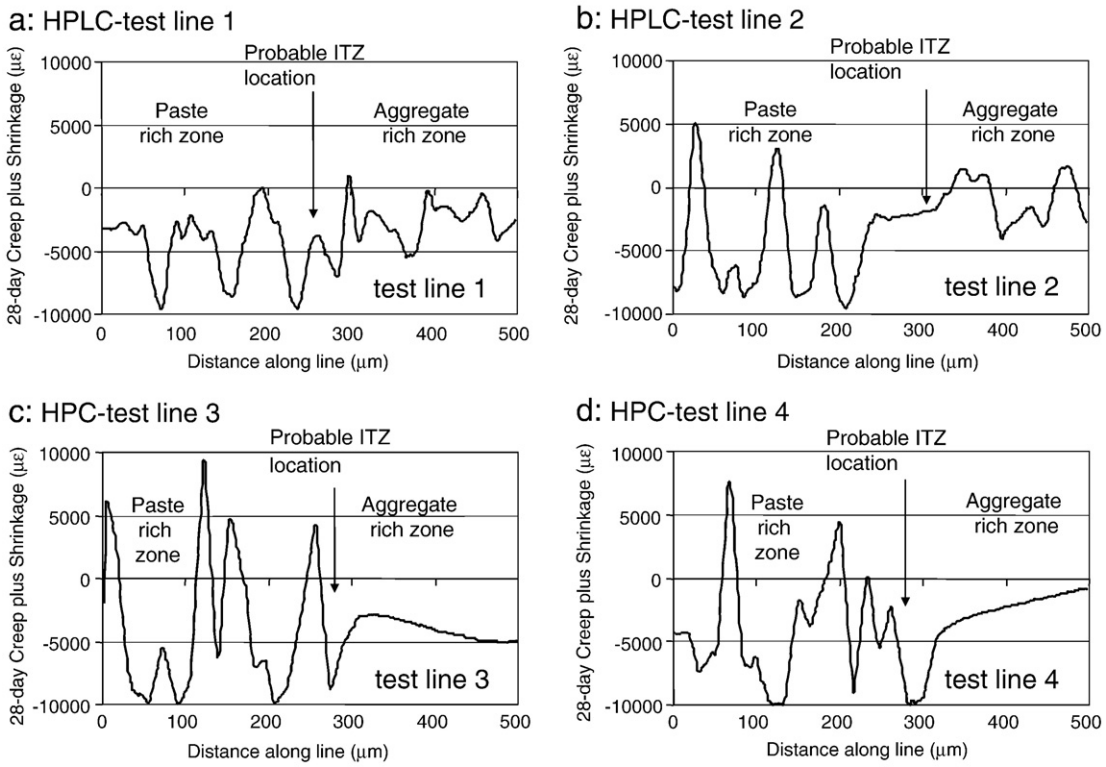

Fig. 7. (a, b). Strain profiles along test lines 1 and 2 across aggregate/paste interfacial region in HPLC. (c, d). Strain profiles along test lines 3 and 4 across aggregate/paste interfacial region in HPC.

own and very dissimilar stiffness. This difference between deformations in the aggregate and in the paste might have induced microcracking at the aggregate/paste interfacial region, as suggested by Fig. 6b.

These results from the elastic strain maps are well explained by the differences between the stiffness of the paste and that of lightweight or granite aggregate. The elastic modulus at the age of 24 h of the high performance paste used in both HPLC and HPC was 35.3 GPa (5165 ksi) [21]. Previous studies [6,33] have reported elastic modulus of granite to be above 70 GPa (10,150 ksi) and that of expanded slate to be below 16.8 GPa (2426 ksi). Thus, the relatively high stiffness of granite might act as a "hard inclusion" causing damage in the aggregate/paste interfacial region during elastic deformations, which was exemplified by the high strain observed in Fig. 6b. On the contrary, the relatively low stiffness of the lightweight aggregate does not impose measurable damage in the paste, as reflected in Fig. 3b. These results agree with the work of Moon et al. [34] that modeled the stress/strain concentration and their effect in cracking of the aggregate stiffness and volume; they found that for unrestrained concrete cracks develop severely as the aggregate stiffness increases. The use of a lower stiffness lightweight aggregate reduce overall concrete stiffness, as shown by the differences in the 24-hour elastic moduli of HPLC and HPC which were 29.1 and 31.9 GPa (4224 and 4630 ksi), respectively.

4.2. Creep and shrinkage strain

Lower creep plus shrinkage strains in concrete with some lightweight aggregates with respect to comparable mixtures with normal weight aggregate have been observed previously [19,20,35,36]. To the authors' knowledge, this is the first study relating this observation to spatial strain distribution across microstructural features in HPC and in concrete containing lightweight aggregate.

The average strain from the creep plus shrinkage maps in HPC were ~16% higher than those obtained from the HPLC strain maps at the same time of testing and level of magnification. This agrees with the results obtained using traditional DEMEC measuring techniques on these samples, as presented above. Similar results have also been obtained by standard creep and shrinkage measurements on HPLC and HPC [9,17]. The results obtained herein also agree with the trends shown by ACI213-R [20]. The image mapping, however, provides additional insight into the underlying mechanisms contributing to the variations in creep behavior in these two high-performance cementitious systems. For both HPLC and HPC, creep and shrinkage deformation occurred as non-uniform strain fields across the concrete microstructure, as revealed by the strain maps.

Furthermore, the strain maps show creep and shrinkage deformations, in both HPLC and HPC, to be more concentrated in the paste-rich regions. The lower time-dependent deformations exhibited by the aggregate with respect to the paste might support the hypothesis [13,14] that the aggregate helps to decrease the creep plus shrinkage of the paste by restraining the deformation in the nearby paste. Accordingly, the restraining effect of the aggregate should increase as the stiffness of the aggregate increases. This, however, was not confirmed by the strain maps and bulk strain data obtained herein. HPLC with a lower stiffness coarse aggregate (expanded slate) showed lower creep plus shrinkage than HPC with a higher stiffness coarse aggregate (granite). This suggests that additional mechanisms affect the creep and shrinkage behavior observed in HPLC.

To further examine the influence of the lightweight aggregate on creep and shrinkage deformation, the behavior near the aggregate/paste interface was examined in both types of concrete. To compare the 28-day creep plus shrinkage strain at the aggregate/paste interfacial region in HPLC and HPC, four straight lines (shown as two solid lines in each ROI of Figs. 3a and 6a) were drawn across the interface at random locations. The strain profiles obtained along each 500-μm long straight line are shown in Fig. 7. Test lines 1 and 2 are from the HPLC interface and test lines 3 and 4 from the HPC.

The creep plus shrinkage strain profile along test line 1 in the HPLC ROI (Fig. 7a) shows relatively similar behavior when comparing the strain variations in paste-rich zone (to the left) and aggregate-rich zone (to the right). However, the strain in the paste-rich zone presents

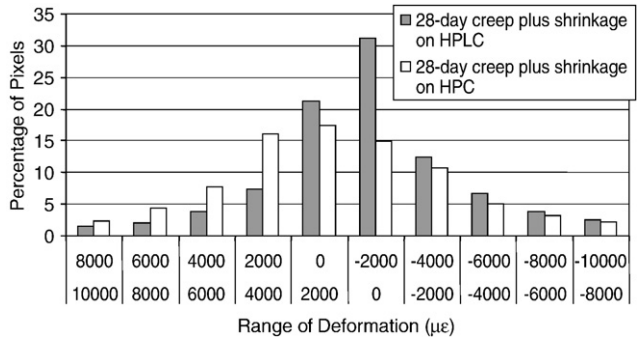

Fig. 8. Strain distribution after 28 days under loading and drying in HPLC and HPC.

more values close to −10,000 με maximum measured and sharper variations in strain with location, than the aggregate. When analyzing the strain at the probable ITZ location (determined from the image itself), it can be noted that there is no comparatively high strain values associated with the transition between aggregate and paste. That is, the strain profile gives no evidence of a measurable strain mismatch between aggregate and paste that might have caused strain concentrations and subsequent cracking in the HPLC in this region.

The creep plus shrinkage strain profile along test line 2 (Fig. 7b), also in the HPLC specimen, shows greater differences between aggregate and paste-rich zones than the profile for test line 1. The paste-rich zone shows sharper changes (greater variability) in strain, with values between +5000 με and −10,000 με, while the aggregate-rich zone presented strains in a narrower range between +1000 με and −5000 με approximately. Despite these differences, similar strain values occurred at the aggregate/paste interface. This suggests that the lower-stiffness, lightweight aggregate reduced strain concentration at the interface, possibly preventing microcracking. The lack of distinct strain behavior at the interface in HPLC could be further explained by the enhanced hydration and subsequent reduction in creep and shrinkage afforded by the use of pre-wetted lightweight aggregate [2,18].

For comparison, peak deformations occurred at the interface in HPC, as shown in the strain profiles of test lines 3 and 4 (Fig. 7c and d). Those profiles show strain mismatch between paste and aggregate at the probable ITZ location. For example, in test lines 3 and 4, variations in strain as large as 7500 and 13,000 με approximately were measured along lengths as short as 30 μm, indicating considerable strain concentrations near the aggregate/paste interface. These measurements of high-strain at the aggregate/paste interface in HPC could partially explain the higher overall creep plus shrinkage measured in HPC with respect to HPLC using image analysis and DEMEC gauges.

Furthermore, the paste-rich zones in the HPC showed higher average creep plus shrinkage and greater extremes in the strain measured, compared to the paste present in HPLC along the test lines. One phenomenon partially explaining the reduced strains in HPLC with respect to HPC is the internal curing provided by the water within the pre-wetted lightweight aggregate [9]. This internal curing may result in microstructural densification within the HPC paste which may also contribute to the lower strain heterogeneity observed in the paste in HPLC.

The strain distribution may be compared for HPLC and HPC after 28 days using the strain maps in Figs. 3c, and 6c. Fig. 8 presents the frequency plot for the data, which shows that, approximately 70% of the matched pixels, in both HPLC and HPC, experienced strains within ±4000 με. However, a clear difference between strain distribution of HPLC and HPC was apparent. Greater homogeneity in strain value distribution was apparent in the HPLC, with 31% of the pixels were concentrated in the range between 0 and −2000 με. In HPC, in contrast, greater scattering of strain values was apparent. In addition, a higher pixel concentration was measured in high tensile levels (e.g., >+6000 με) in HPC than in HPLC. Finally, the standard deviation for HPC was 17,347 με while that of HPLC was 5717 με.

Therefore, it is proposed that the greater consistency in creep plus shrinkage strain measured for HPLC is a consequence of the enhanced strain compatibility between paste and lightweight aggregate, as evidenced by the lower heterogeneity in the strain maps and strain data. The aggregate/paste compatibility in HPLC would reduce stresses at the aggregate/paste interface region, limiting microcracking in the interfacial region. Additionally, the internal curing could have enhanced hydration in the paste near the pre-wetted lightweight aggregate, locally reducing creep and shrinkage. It is also proposed that the lack of highly heterogeneous deformation at the aggregate/paste interface resulted in decreased overall creep plus shrinkage strain in HPLC.

5. Conclusions

Elastic deformations occurred non-uniformly throughout the HPLC and HPC microstructures. However, unlike the mixture with normal weight aggregate (i.e., HPC) which showed strain distribution strongly affected by microstructure (i.e., aggregate, paste and aggregate/paste interface), lightweight aggregate and paste in HPLC deformed similarly, due to enhanced elastic compatibility between the two phases.

The improved strain matching between lightweight aggregate and high performance paste was also observed for the creep plus shrinkage deformations where the strain at the aggregate/paste interface region were noticeably reduced in HPLC as compared to HPC.

Both aggregates (expanded slate in HPLC and granite in HPC) and their surrounding high-performance pastes experienced time-dependent deformation. However, strain maps showed that creep plus shrinkage strains were more concentrated in the paste-rich zones than in the aggregate for both types of concrete when loaded at early age, meaning that the origin of creep and shrinkage is in the high performance paste, as anticipated by creep and shrinkage mechanisms and models [37–39]. Nevertheless, aggregate showed time dependent deformations which are, most probably, related to a delayed elastic deformation rather than creep and shrinkage of the aggregate itself. That is, as the high performance paste underwent creep and shrinkage, it transferred the stresses to the aggregate which gradually exhibited greater elastic deformation.

It is proposed that the observations of transfer of strain from the paste to the aggregate phase demonstrate the current understanding that aggregate restrains creep plus shrinkage occurring in the paste. Based on the data obtained herein for a normal weight and a lightweight aggregate, an aggregate's stiffness may not fully represent its ability to restrain creep and shrinkage deformation in the paste. That is, despite its lower stiffness, expanded slate aggregate more efficiently reduces creep plus shrinkage deformations occurring in the high performance paste than the normal weight aggregate. The decreased creep plus shrinkage showed by the concrete with expanded slate might be in part explained by the reduction of deformation at the aggregate/paste interfacial region as a result of improved bonding, strain compatibility, and also by the improvements in the microstructure at the aggregate/paste interface afforded by the use of pre-wetted lightweight aggregate (i.e., internal curing) as suggested by other study [9].

This examination — using strain maps which allow for spatial correlation between deformation patterns and microstructure — provide evidence that the greater compatibility in the constituent material properties in HPLC allowed for reduction of deformations in the aggregate/paste interfacial region, limiting microcracking and reducing elastic strain and creep plus shrinkage.

Acknowledgements

The authors gratefully acknowledge the research support from the Georgia Department of Transportation under Georgia DOT research project no. 2041, Task Order no. 02-06. The conclusions expressed

herein are those of the authors and do not necessary represent the opinions or conclusions of the Georgia Department of Transportation. The insights given by Dr. Arun Gokhale and the help of Alan Mullenix with the setup are greatly appreciated.

References

[1] T.W. Bremner, Influences of Aggregate Structure on Low Density Concrete, University of London, 1981, p. 229.
[2] M. Lopez, L.F. Kahn, K.E. Kurtis, Internal curing in high performance concretes — a new paradigm (in Spanish), Revista Ingenieria de Construccion 20 (2) (2005) 117–126.
[3] D.P. Bentz, K.A. Snyder, Protected paste volume in concrete — extension to internal curing using saturated lightweight fine aggregate, Cement and Concrete Research 29 (11) (1999) 1863–1867.
[4] P. Lura, O.M. Jensen, S.I. Igarashi, Experimental observation of internal water curing of concrete, Materials and Structures 40 (2) (2007) 211–220.
[5] K. Kovler, O.M. Jensen (Eds.), Internal Curing of Concrete: State-of-Art Report of RILEM Technical Committee 196-ICC: Report 41, RILEM Publications S.A.R.L., Bagneux, 2007, p. 141.
[6] T.W. Bremner, T.A. Holm, Elastic compatibility and the behavior of concrete, Journal of the American Concrete Institute 83 (2) (1986) 244–250.
[7] S. Weber, H.W. Reinhardt, A new generation of high performance concrete: concrete with autogenous curing, Advanced Cement Based Materials 6 (2) (1997) 59–68.
[8] K. Kohno, T. Okamoto, Y. Isikawa, T. Sibata, H. Mori, Effects of artificial lightweight aggregate on autogenous shrinkage of concrete, Cement and Concrete Research 29 (4) (1999) 611–614.
[9] M. Lopez, L.F. Kahn, K.E. Kurtis, Effect of internally stored water on creep of high-performance concrete, ACI Materials Journal 105 (3) (2008) 265–273.
[10] M.D.A. Thomas, Chloride diffusion in high-performance lightweight aggregate concrete, 7th CANMET/ACI International Conference on Durability of Concrete, SP-234, CANMET-ACI, Montreal, 2006.
[11] M.H. Zhang, O.E. Gjorv, Microstructure of the interfacial zone between lightweight aggregate and cement paste, Cement and Concrete Research 20 (4) (1990) 610–618.
[12] M.H. Zhang, O.E. Gjorv, Penetration of cement paste into lightweight aggregate, Cement and Concrete Research 22 (1) (1992) 47–55.
[13] A.M. Neville, Creep of concrete as function of its cement paste content, Magazine of Concrete Research 16 (46) (1964) 21–30.
[14] G. Pickett, Effect of aggregate on shrinkage of concrete and hypothesis concerning shrinkage, Journal of the American Concrete Institute 27 (5) (1956) 581–590.
[15] A. Bentur, S. Igarashi, K. Kovler, Prevention of autogenous shrinkage in high-strength concrete by internal curing using wet lightweight aggregates, Cement and Concrete Research 31 (11) (2001) 1587–1591.
[16] L.F. Kahn, M. Lopez, Prestress losses in high performance lightweight concrete pretensioned bridge girder, PCI Journal 50 (5) (2005) 84–94.
[17] M. Lopez, L.F. Kahn, K.E. Kurtis, Creep and shrinkage of high-performance lightweight concrete, ACI Materials Journal 101 (5) (2004) 391–399.
[18] M. Lopez, K.E. Kurtis, L.F. Kahn, Pre-wetted lightweight coarse aggregate reduces long-term deformations of high performance lightweight concrete, 7th CANMET/ACI International Conference on Durability of Concrete, SP-234, CANMET – ACI, Montreal, 2006.
[19] A.U. Nilsen, P.C. Aïtcin, Properties of high-strength concrete containing light-, normal- and heavy-weight aggregate, Cement Concrete and Aggregates 14 (1) (1992) 8–12.
[20] ACI Committee 213, Guide for structural lightweight-aggregate concrete, ACI Manual of Concrete Practice, American Concrete Institute, Farmington Hills, MI, 2003, p. 38.
[21] M. Lopez, Creep and shrinkage of high performance lightweight concrete a multi-scale investigation, School of Civil and Environmental Engineering, Georgia Institute of Technology, Atlanta, GA, 2005, p. 531.
[22] M. Lopez, L.F. Kahn, K.E. Kurtis, Characterization elastic and time-dependent deformations in normal strength and high performance concrete by image analysis, Cement and Concrete Research 37 (8) (2007) 1265–1277.
[23] ASTM C 109, Standard Test Method for Compressive Strength of Hydraulic Cement Mortars (Using 2-in or [50-mm] Cube Specimens), American Society for Testing and Materials, West Conshohocken, PA, 2002.
[24] C. Videla, M. Lopez, Influence of lightweight aggregate intrinsic strength on compressive strength and modulus of elasticity of lightweight concrete, Revista Ingenieria de Construccion 15 (1) (2000) 43–57.
[25] C. Videla, M. Lopez, Mixture proportioning methodology for structural sand-lightweight concrete, ACI Materials Journal 97 (3) (2000) 281–289.
[26] ASTM C 512, Standard Test Method for Creep of Concrete in Compression, American Society for Testing and Materials, West Conshohocken, PA, 2002.
[27] Matrox-Imaging, Matrox Inspector 4.1. 2002.
[28] S. Choi, S.P. Shah, Measurement of deformations on concrete subjected to compression using image correlation, Experimental Mechanics 37 (3) (1997) 307–313.
[29] C.M. Neubauer, H.M. Jennings, The use of digital images to determine deformation throughout a microstructure — part II — application to cement paste, Journal of Materials Science 35 (22) (2000) 5751–5765.
[30] C.M. Neubauer, H.M. Jennings, E.J. Garboczi, Mapping drying shrinkage deformations in cement-based materials, Cement and Concrete Research 27 (10) (1997) 1603–1612.
[31] F.G. Thomas, Creep of Concrete under Load, International Association of Testing Materials, London, 1937.
[32] A.M. Neville, W.H. Dilger, J.J. Brooks, Creep of Plain and Structural Concrete, Construction Press, 1983.
[33] M.G. Alexander, Aggregate and the deformation properties of concrete, ACI Materials Journal 93 (6) (1996) 569–577.
[34] J.-H. Moon, F. Rajabipour, B. Pease, J. Weiss, Autogenous shrinkage, residual stresses, and cracking in cementitious composites: the influence of internal and external restraint, Self-Desiccation and Its Importance in Concrete Technology, Lund University Lund Institute of Technology, Gaithersburg, Maryland, USA, 2005.
[35] D.W. Pfeifer, Sand replacement in structural lightweight concrete — creep and shrinkage studies, American Concrete Institute — Journal 65 (2) (1968) 131–140.
[36] G.L. Rogers, On the Creep and Shrinkage Characteristics of Solite Concretes, Proceedings of World Conference on Prestressed Concrete, University of California in Cooperation with the Prestressed Concrete Institute, 1957, San Francisco, CA, pp. 2.1–2.5.
[37] A.M. Neville, Theories of creep in concrete, ACI Journal 52 (1955) 47–60.
[38] A.M. Neville, Role of cement in creep of mortar, Journal of the American Concrete Institute 30 (9) (1959) 963–984.
[39] Neville, A.M. and W.H. Dilger, Creep of concrete: plain, reinforced, and prestressed. 1970, Amsterdam, New York,: North-Holland Pub. Co. American Elsevier. xix, 622.